Bio-synthesis of gold nanoparticles from Codariocalyx motorius leaf extract: Physiochemical evaluation, antimicrobial, antioxidant and anticancer activity against Hep G2 cell lines

Saravana Kumar Deivanathan
Government Arts College, (Affiliated to Bharathidasan Univerity, Tiruchirappalli-24) Tiruchirappalli - 620 022.
B. Mary Dayana
St. Joseph's College (Autonomous), (Affiliated to Bharathidasan University, Tamil Nadu)
J. Thomas Joseph Prakash (armyjpr1@yahoo.co.in)
Government Arts College, (Affiliated to Bharathidasan Univerity, Tiruchirappalli-24) Tiruchirappalli - 620 022.

Research Article

Keywords: Codariocalyx motorius, gold nanoparticles, antibacterial, antifungal, anti-oxidant, Hep G2 cell lines

Posted Date: October 27th, 2023

DOI: https://doi.org/10.21203/rs.3.rs-3468468/v1

Additional Declarations: No competing interests reported.

Abstract

This research delved into the synthesis of gold nanoparticles (AuNPs) utilizing leaf extract derived from *Codariocalyx motorius (C.motorius)*. The confirmation of *C.motorius* gold nanoparticles (CM-AuNPs) formation was established through the visual observation of color changes in the colloidal solution. A comprehensive characterization of CM-AuNPs employed UV-vis spectroscopy, FT-IR, FE-SEM, EDAX, XRD, HR-TEM, DLZ and Zeta potential. The UV- vis spectrum exhibited a distinctive peak at 534 nm, indicative of CM-AuNPs. The FT-IR spectrum identified the presence of -OH and -NH functional groups intricately associated with the AuNPs. HR-SEM analysis revealed average size of approximately 44 nm for the CM-AuNPs. XRD confirmed the face-centered cubic crystallinity of CM-AuNPs. In the DPPH assay, the bio-synthesized CM-AuNPs demonstrated robust antioxidant activity, displaying an IC_{50} of 61.27%. Moreover, the bio-synthesized CM-AuNPs exhibited significant antibacterial efficacy against both gram-positive (*Staphylococcus aureus*) and gram-negative (*Escherichia coli*) bacteria. Inhibition values for these bacteria were recorded at 6 ± 2.94392 mm and 5 ± 2.58199 mm respectively. Further, the bio-synthesized AuNPs showcased antiproliferative activity against Hep G2 cells, with an IC_{50} value 6.89 µg/mL. These compelling findings underscore the potential applications of CM-AuNPs, synthesized from *C.motorius* leaf extract in the realm of medication delivery.

Introduction

Nanotechnology is an innovative field at the forefront of scientific and technological progress, focusing on the manipulation and control of matter on an incredibly minute scale. Researchers delve into the nanoscale, typically ranging from 1 to 100 nanometers, to unlock a wide range of exceptional properties and phenomena [1]. This discipline revolves around comprehending and harnessing the characteristics of the materials at this scale, where they exhibit novel attributes arising from quantum effects and an augmented surface-to-volume ratio. Consequently, nanotechnology holds immense potential to revolutionize diverse industries [2], including electronics [3], medicine [4], energy and environmental sciences [5]. At the nanoscale, materials can be deliberately engineered, manipulated and precisely assembled to generative new functionalities. Such manipulation is guided by the principles of quantum mechanics, enabling the exploration of quantum phenomena and the development of remarkable technologies with unparalleled capabilities. Although still in its early stages, the field of nanotechnology is expanding rapidly. As scientists and engineers deepen their understanding of nanoscale matter manipulation [6–8].

In the realm of cancer diagnosis and treatment silver (Ag), gold (Au) stands as common stalwarts. The impact of oxide and metal nanoparticles on cellular toxicology hinges on their concentration, dimension, structural configuration and surface characteristics [9]. It's noteworthy that an augmentation in surface charge amplifies the toxicity of nanoparticles. Detecting the cancer in its early stages offers patients a significantly greater chance of a successful cure before it spreads to other parts of the body [10]. Current cancer treatment approaches encompass surgery, radiation therapy and other modalities. Chemotherapy, while effective at targeting rapidly dividing cancer cells, also impacts healthy cells as those in the bone marrow and the immune system, resulting in significant collateral damage to the patient's overall health [11]. Moreover, sorafenib, an DA -approved medication for advanced liver cancer, demonstrate limited efficiency in terms of patient survival. Research reveals that in the group receiving sorafenib treatment, the overall survival rate was 10.7 months as compared to 7.9 months in the placebo group. This marginal difference suggests only a slight extension inpatient survival due to sorafenib treatment. Additionally, conventional treatments like chemotherapy and radiotherapy have proven ineffective in addressing Hep G2 cancer [12, 13].

Traditional techniques utilized in the synthesis of gold nanoparticles (AuNPs) frequently entail the utilization of hazardous substances and costly methodologies, thereby accentuating environmental hazards and impending its clinical application despite its captivating attributes [14]. Hence, the exploration of a straightforward, environmentally

friendly and economically viable approach becomes a significant imperative. In recent times, the utilization of fungi, algae and plant crude extracts as a green pathway for synthesizing AuNPs has garnered substantial interest from researchers, owing to its non-toxic and eco-friendly characteristics [15].

Codariocalyx motorius (C.motorius) commonly known as “Dancing Plant” or “Telegraph Plant” is a fascinating and unique species in the plant kingdom. Native to Southeast Asia and other tropical regions, this plant belongs to the Fabaceae family and is known for its distinctive ability to exhibit rapid and visible leaf movement, resembling a dance or a response to external stimuli. The rapid leaf movement of *C.motorius* has attracted the attention of scientists and researchers interests in understanding the mechanics of plant movement and tropism. Studying this plant’s responses to various stimuli has provided valuable insights into physiology and cellular biology. In some traditional medicine practices, parts of the *C.motorius* plant have been used for their potential medicinal properties, although scientific evidence supporting these claims is limited.

In our research project, we achieved the synthesis of gold nanoparticles (AuNPs) that are environmentally friendly, cost-efficient, non-toxic and safe for the environment. We utilized *C.motorius* leaf extract (CMLE) as a natural reducing agents in the production process. To assess the characteristics of these AuNPs, we conducted a comprehensive analysis using various techniques including UV-visible spectroscopy, X-Ray diffraction (XRD), Fourier-transform infrared spectroscopy (FT-IR), FE-SEM (Field emission scanning electron microscopy) with energy-dispersive X-ray analysis (EDAX), high resolution tunneling electron microscopy (HR-TEM), selected area electron diffraction (SAED), dynamic light scattering (DLS) and Zeta potential measurement.

We also, evaluated the antimicrobial properties of these bio-synthesized AuNPs using disc diffusion method. Additionally, we conducted examinations to determine their antioxidant properties and anti-cancer activity against Hep G2 Liver cancer cell lines.

Materials and methods

Chemicals and materials

The *Codariocalyx motorius* plants were collected from Kolli hills, Namakkal District, Tamil Nadu, South India. HAuCl4 (Gold (III) chloride trihydrate, also known as chloroauric acid, was purchased from sigma-Adrich. This compound was used as a gold precursor in the study. All Solutions were prepared with aqua pure double distilled water and stored in the dark to prevent photochemical reactions. Glassware used in the experiments was cleaned with a solution acetone, rinsed thoroughly with double-distilled water and dried before use.

Preparation of CMLE

The freshly collected leaves of *C.motorius* underwent a meticulous cleansing process involving dual rinsing with aqua pure double distilled water, ensuring the elimination of dust and undesirable adhering to the leaf surfaces. Subsequently, these pristine leaves were left desiccate naturally under ambient temperature under the shadow. Following this, the desiccated leaves were meticulously minced into diminutive fragments. A 2 g of these finely chopped dried leaf fragments was transferred into 200 mL of beaker, contains 100 mL of water. The mixture was heated until the pungent smell and then allowed to cool. The boiled mixture solution was carefully filtered through Whatman No.1 filter paper. To preserve this, the filtrate was stored in a refrigerator at 4 ºC for further characterization studies.

Bio-synthesis of CM-AuNPs

The bio-synthesis approach was employed to produce gold nanoparticles (AuNPs) by reducing 1 mM chloroauric acid ($HAuCl_4$) using *C.motorius* leaf extract. A 1 mM solution of gold (III) chloride ($HAuCl_4$) was meticulously combined with CMLE and the resulting was carefully poured into a 200 mL beaker a ratio of 2:8 and the mixture underwent vigorous stirring by magnetic stirrer for a duration of an hour. Throughout the speed, the transformation of the solution's color was meticulously observed, revealing a discernible divergence from its initial state. The resultant biosynthesized AuNPs solution underwent a ten-minute centrifugation process at an impressive 12,000 revolution per minute using Remi 12C machine. To facilitate the swift and seamless transformation into powdered form, the substance was subjected to a heated air furnace, maintaining temperature of approximately 100 ºC for a duration of 10 minutes. Following this, the desiccated CM-AuNPs powder underwent a comprehensive analysis to ascertain their characteristics.

Characterization studies

The process of bio-synthesized $HAuCl_4$ into AuNPs utilizing *C.motorius* was diligently monitored at regular basis, using UV-vis spectrometer (Perkin Elmer Model: lamba 35) with an extensive wavelength range from 190–1100 nm. To unravel the functional groups and associated bonds present in the synthesized sample, FT-IR analysis (Perkin Elmer) was conducted, exploring the frequency range from 400 cm^{-1} to 400 cm^{-1}. Employing the DLS method, an examination of the hydrodynamic dimension of the nanoparticles within the material was performed. This was achieved through the utilization of the Malvern PAnalytical Nano Zs instrument, which encompassed a scope of 0.1 nm to 12.3 µm, providing insight into the Zeta potential of the synthesized AuNPs. Furthermore, the crystallinity of the bio-synthesized AuNPs was elucidated through X-ray diffraction investigation employing the PAnalytical Xpert Plus instrument. XRD analysis was employed to determine the powdered AuNPs utilizing a CuK radiation with a wavelength (λ) of 1.54nm and a scanning angle (2θ) ranging from 10º to 80º. The investigation of surface morphology EDAX (energy dispersive X-ray Spectroscopy) configuration was employed by Field Emission Scanning Electron microscope (FE-SEM) with FEI 250 model. On the other hand, HR-TEM utilized JEOL 2100 + model, renowned for its superior performance in particle size analysis. For the generation of comprehensive visual representation, including X-ray diffraction (XRD) patterns, FT-IR, Ultraviolet (UV) spectra, error maps and histograms, Origin 2018 software was employed.

Anti-microbial activities

To access the bacterial efficacy of different samples, a disc diffusion assay was employed. This assay entails filling 60 mm petri dishes with Mueller-Hinton agar (MHA) and inoculating them with bacteria. Subsequently, these nutrient-rich plates were inoculated with bacteria. To investigate the antimicrobial potential of the various samples, small sterile discs, exhibiting a diameter of 60 mm, were delicately impregnated with 10 µL of each specimen. These soaked discs were then cautiously positioned atop the agar plates, allowing a duration of 30 minutes at ambient temperature for the compounds present in the samples to diffuse uniformly. In order to establish a positive control, a disc saturated with 10 µL of Amoxicillin, a widely utilized antibiotic was included. The plates, thus prepared were included at a thermostatically controlled temperature of 37 ºC for a period of 24 h, fostering an optical environment for bacterial growth. Subsequently, the diameter of the distinct transparent zones surrounding each disc, renowned as the zone of inhibition was meticulously measured in mm. in order to ensure precision and veracity of results, this experimental procedure was diligently replicated twice.

Antioxidant assay

The antioxidant properties of the synthesized AuNPs were assessed using the stable DPPH free radical scavenging assay. A solution of DPPH in ethanol with a concentration of 0.05 mM was prepared and combined with 1000 µL of

bio-synthesized nanoparticles at various concentrations ranging from 20–100 µL. The freshly prepared DPPH solution was stored in darkness at a 4 ºC. Subsequently, 2.7 mL of 96% ethanol was added to the mixture and vigorously stirred. The resulting mixture was left undisturbed for 5 minutes, after which the absorbance was measured using spectrophotometry at a wave length of 540 nm. In order to account for any inherent absorbance, a control sample consisting of the same amount of ethanol and DPPH was prepared. All measurements were conducted three times to ensure the accuracy. The DPPH free radical activity of the samples was quantified as the percentage of inhibition using the formula:

Inhibition % = = $\frac{A-B}{A}$ ×100

Here, A represents the absorbance value of the blank, and B represents the absorbance value of the sample. A graph subsequently constructed to illustrate the relationship between the concentration of the sample and the corresponding percentage of inhibition. By analyzing the graph, the concentration required to 50% value of inhibition was determined.

Cytotoxicity assay

A cell viability of assay was performed using Hep-G2 cells. They were harvested and counted using haemocytometer. They were, then diluted in DMEM medium to a density of 1×104 cells/mL. The cells were seeded in 96-well plates, allowing them to attach for 24 h. Following this, different concentration of biosynthesized AuNPs (ranging from 2.5 to 15 µg/mL) were applied to each well, along with a control group. The plates were then incubated at 37 ºC in a humidified environment containing 95% air and 5% CO_2 for 24 h. After the incubation period, the drug-containing cells were washed with fresh culture medium. MTT dye (5 mg/mL in PBS) was added to each well and the plates were further incubated for 4 h at 37 ºC. The purple precipitate, formazan formed as a result. To measure cell viability, the formazan was dissolved in 100 µL of concentrated DMSO and the absorbance was measured at 540 nm using a multi-well plate reader. The results were expressed as the percentage of viable cells relative to the control group. The half maximal inhibitory concentration (IC_{50}) values were calculated and the optimal doses were analyzed at different time intervals.

$$\mathrm{Inhibitoryofcellproliferation}\ (\%) = \frac{\mathrm{Meanabsorbenceofthecontrol} - \mathrm{Meanabsorbenceofthesample}}{\mathrm{Meanabsorbenceofthecontrol}} \mathrm{X100}$$

The IC_{50} values were obtained by analyzing the dose response curve of AuNPs, which indicated the concentration at which 50% cytotoxicity was observed compared to the control cells. To ensure accuracy, the experiments were conducted a minimum of three times, with each experiment performed in triplicate.

Result and discussion

UV- Vis spectroscopical analysis of CM-AuNPs

The Fig. 1 depicts the result of the UV-vis spectroscopic analysis conducted on CM-AuNPs. Over time, as the reaction proceeds, a greater number of Au ions undergo conversion of Au nanoparticles, resulting in a more concentrated and vivid coloration of the gold solution [16]. The UV- vis spectra findings serve as an indirect yet highly effective means of discerning the emergence of nanoparticles. To track the advancement of the reaction leading to the transformation of Ag^+ from $AgNO_3$ into reduced nano silver, the alteration in color and the peak absorbance maxima with in the wavelength range of 514–550 nm were carefully monitored [17]. Notably, a prominent peak appeared at 529 nm, with no additional peaks detected in this specific region, signifying the formation of well-dispersed gold nanoparticles with

in the reaction medium. This particular band at 529 nm corresponds to the surface plasmon resonance (SPR) characteristics exhibited by AuNPs [18, 19].

FT-IR analysis of bio-synthesized CM-AuNPs

Subsequently, an FT-IR analysis was conducted on CM-AuNPs, and the corresponding spectra are depicted in Fig. 2. Four distinct peaks were observed in the CM-AuNPs spectrum, specially at 3344 cm^{-1}, 2890 cm^{-1}, 2111 cm^{-1} and 1634 cm^{-1}. The broad peak detected at 3344 cm^{-1} can be attributed to the presence of O-H bonds, originating from alcohol and phenolic groups [17]. The peak at 2890 cm^{-1} signifies the stretching vibrations of the -CH groups in alkanes [20], while the peak at 2111 cm^{-1} corresponds to N-H bonding and C = O stretching vibrations in proteins [21]. Furthermore, the vibrations observed at 1634 cm^{-1} is indicative of the C-C stretching in aromatic rings, confirming the presence of an aromatic group [22, 23]. These byproducts, namely alcohol, phenolic compounds, alkanes and proteins are responsible for the reduction of Au^{+} ions to Au^{0} metal nanoparticles [24].

Powder XRD analysis of bio-synthesized CM-AuNPs

To determine the crystalline nature and purity of the synthesized AuNPs, X-ray diffraction analysis was conducted and the results are presented in Fig. 3. Notable diffraction peaks were observed at 38.34º, 44.53º, 64.75º and 77.73º in 2θ values, corresponding to the (111), (200), (220) and (311) lattice planes respectively of the face centered cubic structure of AuNPs. Among these planes, the (111) plane exhibit the highest peak intensity, indicating its prominence over the others. No additional discernible peak observed. Confirming the purity of the synthesized AuNPs. These findings align well with the JCPDS file no (04-0784) and the previous studies [25–28].

Furthermore, the average particle size was determined using Scherrer's equation,

Average crystalline size = $\frac{k\lambda}{\beta cos\theta}$

Where, k is a constant, λ is the wavelength (λ = 1.5406 Å) β is the full width at half maximum (FWHM) of the high-intensity plane and θ is Bragg's angle. The estimated average crystalline size of the bio-synthesized AuNPs was calculated to be 24 nm.

FE-SEM analysis of CM-AuNPs.

The surface morphology analysis of bio-synthesized AuNPs using FE-SEM as shown in the Fig. 4. The FE-SEM images revealed the presence of spherical nanoparticles consists with the observation from transmission electron microscope (TEM) images. Furthermore, we confirmed the presence of AuNPs through EDAX analysis as illustrated in the Fig. 4. In the EDAX spectrum, a distinct gold signal was detected at 2.0 keV [29], which was serves as a clear indicator of the presence of AuNPs. It's worth noting that the spectra also exhibited Oxygen peaks, likely stemming from the interaction of biomolecules with the surface of the AuNPs detectable at 0.4 keV [30].

HR-TEM analysis of CM-AuNPs

The HR-TEM images of the bio-synthesized AuNPs using extract from *C.motorius* plant exhibit poly-dispersed nanoparticles with spherical shape as depicted in Fig. 5. The majority of AuNPs synthesized from CMLE displayed a spherical morphology. These spherical particles exhibited a remarkable degree of uniformity the average size of the bio-synthesized CM-AuNPs is 44 nm. These findings align with prior research that has consistently shown that spherical nanoparticles tend to have smaller dimensions compared to other morphological variant as reported in studies. [31–33]

Zeta potential and DLS analysis of CM-AuNPs

Zeta potential represents the electrical potential difference between the mobile solvent and the stationary layer of the solvent attached to the dispersed nanoparticles. The surface charge of the nanoparticles is a crucial characteristic that plays a significant role in determining their colloidal stability, structure and overall functionality [34]. In this study, the surface of the bio-synthesized nanoparticles was assessed through zeta potential analysis depicted in Fig. 6. The obtained result revealed a mean zeta potential of -12.6 mV, indicating a high level of stability. The presence of negative zeta potential value can be attributed to the potential existence of capping agent within the extract, which serves to inhibit the aggregation of nanoparticles [35]. The exceptional stability of the AuNPs can be attributed to the robust electrostatic repulsion operating between the particles. These repulsions play a pivotal role in ensuring the long-term stability, favorable colloidal characteristics and excellent dispersity of the nanoparticles [36]. The DLS technique was employed to determine the particle size of the size distribution, revealing a hydrodynamic average particle diameter of gold nanoparticles measured at 124.57 nm (Fig. 6b) and the PDI (poly dispersity index) value of 0.281shows that the particles are moderate poly-dispersed with particle size ranges from 10.2 nm to 238.8 nm. It is worth noting that the particle size obtained through DLS analysis appears to be larger compared to the size observed in HR-TEM image analysis. This variation could potentially be attributed to the presence of capping agents such as ionic liquids and other organic moieties that interact with the nanoparticles [28].

Anti-microbial examination of CM-AuNPs

We conducted an assessment of the antimicrobial properties of CM-AuNPs against various human bacterial pathogens, including *Staphylococcus aureus* (MTCC 25923), *Escherichia coli* (MTCC 25922), *Aspergillus flavus* (MTCC 356) and *candida albicans* (MTCC 227). The inhibition zones surrounding each well are illustrated in the Fig. 7, with corresponding values for the created zones and the antibiotic control Amoxicillin provided for clarity. The inhibition zones for *Staphylococcus aureus*, *Escherichia coli, Aspergillus niger* and *Candida albicans* were determined to be 6 ± 2.94392 mm, 5 ± 2.58199 mm, 3 ± 1.82574 mm and 7 ± 1.82574 mm respectively (**Table No.1**). In contrast, *Aspergillus flavus* (MTCC 356) exhibited a less responsive reaction.

Upon contact with bacterial cells, the bio-synthesized CM-AuNPs, with their size advantage, effectively penetrated the cell wall (Fig. 11) once inside, these nanoparticles interacted with crucial components of bacterial and fungal cells, notably the membrane and enzymes [37]. AuNPs exhibited an affinity for binding to sulfur-containing compounds within the cell membrane and proteins. This interaction compromised the structural integrity of the cell membrane, including permeability loss and functional impairment [38]. The introduction of Reactive Oxygen Species (ROS) played a pivotal role in bacterial cell death. ROS functioned as potent agents disrupting normal cellular functions and triggering cell death. These species targeted and damaged vital biomolecules such as lipids, proteins, and DNA [39].

Table No.1 Anti-microbial analysis of CM-AuNPs

Samples	Concentrations (µL/mL)	Organisms/Zone of inhibition (mm)			
		Staphylococcus aureus[@]	*Escherichia coli*[@]	*Aspergillus flavus*[#]	*Candida albicans*[#]
A (Amoxicillin[@] / fluconazole[#])	10	10 ± 2.94392	13 ± 2.58199	6 ± 1.82574	8 ± 1.82574
	10	0 ± 0	0 ± 0	0 ± 0	0 ± 0
B (Au solution)	10	2 ± 0.8165	3 ± 1.82574	2 ± 1.82574	4 ± 1.82574
C (CM extract)	10	6 ± 2.94392	5 ± 2.58199	3 ± 1.82574	7 ± 1.82574
D (AuNps)					
* At the 0.05 level, the population means are significantly different					

Anti-oxidant analysis of CM-AuNPs

The integration of AuNPs into DPPH analysis represents a sophisticated approach to assessing antioxidant activity. As the realm of nanotechnology continues to expand the utilization of AuNPs in DPPH analysis promises to deeper insights into the antioxidant potential of compounds, fostering innovation and advancement in multiple industries [40, 41]. The investigation into the DPPH radical scavenging activity of AuNPs revealed a clear correlation with both the concentration with both the concentration of standard solution and the bio-synthesized AuNPs. The AuNPs are known for their ability to provide electrons or hydrogen atoms which helps reduce the levels of radical like DPPH. When AuNPs come into contact with DPPH radicals they exchange electrons or hydrogen atoms effectively neutralizing the radicals. [42]. The outcomes demonstrated a significant dose-dependent reduction in DPPH free radicals' concentrations of 20, 40, 60, 80 and 100 µg/mL. The results (**Table No.2**) revealed that bio-synthesized AuNPs have significant antioxidant potential when compared to standard ascorbic acid. The apex of antioxidant activity within the AuNPs containing extract was observed at 100 µg/mL, registering at an impressive 80.39%. The heightened activity could be attributed to the AuNPs' capacity to furnish electrons or hydrogen ions, thus mitigating the impact of DPPH free radicals [43]. As the concentration increased, the radical- scavenging prowess followed suit in a proportional fashion and the IC_{50} of the CM-AuNPs by method is DPPH is 61.27%.

Table No.2 Antioxidant activity of CM-AuNPs by DPPH assay method

S.NO	CONCENTRATION (µg/mL)	ANTIOXIDANT ACTIVITY DPPH%	
		SAMPLE	ASCORBIC ACID
1.	20	35.29 ± 2.98246	50.98 ± 4.39167
2.	40	54.90 ± 5.24598	68.62 ± 3.67707
3.	60	67.64 ± 4.63785	76.47 ± 3.39225
4.	80	73.52 ± 1.85721	82.35 ± 3.68804
5.	100	80.39 ± 1.74102	88.23 ± 5.91275

Anti-cancer analysis against Hep G2 cell lines

AuNPs enter cancer cells via endocytosis or passive diffusion due to their small size and surface charge. Once internalized, AuNPs accumulate within endosome, lysosomes or the cytoplasm depending on their surface properties [44]. The bio-synthesized AuNPs can induce the generation of reactive oxygen species (ROS) within cancer cells, when the ROS produced as a result of AuNPs's action have the capacity to interfere with the proper functioning of mitochondria within liver cancer cells. This disruption of mitochondrial activity can have significant consequences, including the release of cytochrome and activation caspases [45]. These events serve as pivotal triggers for the initiation of apoptotic pathways within the liver cancer cells. More specially, the cumulative impact of ROS accumulation and the mitochondrial dysfunction collaborative activities the apoptotic cascade. This mode of cell demise is marked by noticeable cellular changes (Fig. 9), such as shrinkage [46], DNA fragmentation [47] and membrane blebbing [48]. In this research, when the concentration of the bio-synthesized CM-AuNPs were increased, results a significant change in the Hep G2 liver cell lines (Fig. 10)

Conclusion

In this current research, we successfully pioneered an innovative and environmentally friendly approach for the synthesis of stable AuNPs using *C.motorius* leaf extract. The comprehensive characterization of the AuNPs encompassed assessments of size, surface morphology, surface charge and chemical composition employing techniques such as UV-vis Spectroscopy, XRD, FE-SEM, EDAX, HR-TEM with SAED, DLS and zeta potential. The bio-synthesized CM-AuNPs exhibited a distinctive spherical shape with an average size measuring 44 nm. XRD and SAED analyses provided compelling evidence of the crystalline nature of the bio-synthesized AuNPs. FT-IR analysis corroborated the presence of -OH and -NH groups, which played a pivotal role in the reducing of $HAuCl_4$ to AuNPs. Furthermore, the bio-synthesized CM-AuNPs demonstrated potent DPPH free radical scavenging activity. In-vitro anticancer evaluations revealed that CM-AuNPs exerted significant cytotoxic effects against Hep G2 cancer cell lines. The observed cytotoxicity is attributed to the collaborative action of phenolic moieties and the AuNPs. This noteworthy synergy suggests the potential of bio-synthesized CM-AuNPs as a prospective source for the development of novel antimicrobial and anticancer drugs.

Declarations

Acknowledgement

The author Saravana Kumar Deivanathan express his gratitude to Healer. Selvam Dhanaraju, Valaiyapatti, Thuraiyur, Tiruchirappalli (DST) and Mr. Mohan Raj Gopalakrishnan M.C.A., Software Engineer, Tiruchirappalli, Tamil Nadu, India.

CRediT author statement

Saravana Kumar Deivanathan: Conceptualization, Methodology, Data curation, Writing- Original draft preparation. **B. Mary Dayana:** Software, Validation, Writing- Reviewing and Editing. **J. Thomas Joseph Prakash:** Reviewing and Editing, Visualization, Investigation and Supervision.

Ethical Approval

We also declare that the study was performed according to the international, national and intuitional rules considering animal experiments, clinical studies and biodiversity rights. And also, no animals / humans were harmed in this research work.

Competing interests

The authors declare that they have no competing interest.

Author's contributions

Authors

We confirm that the manuscript has been read and approved by all named authors and that there are no other persons who satisfied the criteria for authorship but are not listed. We further confirm that the order of authors listed in the manuscript has been approved by all of us.

Funding

This research did not receive any specific grant from funding agencies in the public, commercial, or not-for-profit sectors.

Availability of data and materials

The data that support the findings of this study are included within in the article.

Corresponding Author

We understand that the Corresponding Author is the sole contact for the Editorial process. He is responsible for communicating with the other authors about progress, submissions of revisions and final approval of proofs.

Copyright and Plagiarism

We declare that this manuscript is original, has not been published before and is not currently being considered for publication elsewhere.

References

1. S. Ahmed, M. Ahamed, B.L Swami, S. Ikram. J. Adv. Res **7**, 17-28 (2016).
2. S. Paidari, S.A Ibrahim. Gold Bull **54**, 31–36 (2021).
3. I. Hammami, N.M Alabdallah, A.A Jomaa, M. Kamoun. J. King Saud Univ. Sci. **37,** 101560 (2021).
4. F.E Meva, M.L Segnou, C.O Ebongue, A.A Ntoumba, P.B.E Kedi, V. Deli, M.A Etoh, E.M Mpondo. Rev. Bras. Farmacog. **26,** 640-646 (2016).
5. V. Kumar, D.K Singh, S. Mohan, R.K Gundampati, S.H Hasan. J. Environ. Chem. **5,** 744-756 (2017).
6. S. Bayda, M. Adeel, T. Tuccinardi, M. Cordani and F. Rizzolio. Molecules **25,** 112 (2020).
7. W. Mahakham, P. Theerakulpisut, S. Maensiri, S. Phumying, A.K Sarmah. Sci. Total Environ. **573**, 1089-1102 (2016)
8. A.T Singh, I.N Shaikh, M.V Rale. Mater. Today: Proc. **43**, 2805-2809 (2021).
9. A. Mojaddami, Z. Koolivand, M. Panahimehr, N. Chamkouri. Nano-Struct. Nano-Objects. **34,** 100979 (2023).
10. S. Medici, M. Peana, D. Coradduzza, M.A Zoroddu. Semin. Cancer Biol. **76,** 27-37 (2021).
11. Z.Z.J Lim, J.E.J Li, C. Teng NG, L.Y.L Yung. B.H Bay. Acta Pharmacol Sin. **32,** 983–990 (2011).

12. H. Barabadi, T.J Webster, H. Vahidi, H. Sabori, K.D Kamali, F.J Shoushtari, M.A Mahjoub, M. Rashedi, E. Mostafavi, D.M Cruz, O.Hosseini, M. Saravana. Iran J Pharm Res. **19,** 3-17(2020).
13. H.M Ebrahim, E.E Rouby, M.E Morsy, M.M Said, M.K Ezz. Asian Pac J Cancer Prev. **20**, 3369-3376 (2019).
14. K.N Patel, P.G Trivedi, M.S Thakar, K.V Prajapati, D.K Prajapati, G.M Sindhav. J Genet Eng Biotechnol **21,** 71 (2023).
15. T.S.K Sharma, K. Selvakumar, K.U Hwa, P. Sami, M. Kumaresan. J. Mater. Res. **8,** 1412-1418 (2019).
16. D. Nayak, S. Ashe, P.R Rauta, M. Kumari, B. Nayak. Mater. Sci. Eng. C **58,** 44-52 (2016).
17. T. Ahamed, M. Irfan, M.A Bustam, S. Bhattarcharjee. Procedia Eng. **148,** 467-472 (2016). doi: 10.1016/j.proeng.2016.06.465
18. O.S ElMitwalli, O.A Barakat, R.M Daoud, S. Akhtar, F.Z Henari. J Nanopart Res. **22,** 309 (2020).
19. J.S Boruah, C. Devi, U. Hazarika, P.V.B Reddy, D. Chowdhury, M. Barthakur, P. Kalita. RSC Adv **11,** 28029-28041 (2021).
20. J.L Coward. J Biol Phys **36**, 405–425 (2010).
21. C. Chellapandian, B. Ramkumar, P. Puja, R. Shanmuganathan, A. Pugazhendhi, P. Kumar. Process Biochem. **80,** 58-63 (2019).
22. G. Sathishkumar, K.J Pradeep, V. Vignesh, C. Rajkuberan, M. Jeyaraj, M. Selvakumar, R. Jha, S. Sivaramakrishnan. J. Mol. Liq.**215,** 229-236 (2016).
23. B. Paul, B. Bhuyan, D. D Purkayastha, S. Vadivel, S.S Dhar. Mater. Lett. **185,** 143-147 (2016).
24. J.A Aboyewa, N.R.S Sibuyi, M. Meyer, O.O. Oguntibeju. Plants **10,** (2021) 1929.
25. M. Vinosha, S. Palanisamy, R. Muthukrishnan, S. Selvam, E. Kannapiran, S. You, N.M Prabhu. Process Biochem. **85,** 219-229 (2019).
26. Q. Zhou, M. Zhou, Q. Li, R. Wang, Y. Fu, T. Jiao. Colloids Surf. A **567,** 69-75 (2013).
27. S. Vijayakumar, R. Vinayagam, M.A.V Anand, K. Venkatachalam, K. Saravanakumar, M.H Wang, C.S Casimeer, KM Gothandam, E. David. J Drug Deliv Sci Technol. **58,** 101786(2020).
28. R. Khandanlou, V. Murthy, H. Wang. Mater. Sci. Eng. C **112,** 110922 (2020).
29. R. Khandanlou, V. Murthy, D. Saranath, H. Damani. J Mater Sci **5,** 3106-3118 (2015).
30. N. Dorosti, F. Jamshidi. J. Appl. Biomed. **14,** 235–245 (2016).
31. J. John, L. Thomas, A. Kurian, S.D George. J. Lumin **172,** 39-46 (2016).
32. G. Lakshmnan, A. Sathiyaseelan, P.T Kalaichelvan, K. Murugesan. Karbala Int. J. Mod. Sci. **4,** 61-68 (2018).
33. S. Zada, A. Ahmad, S. Khan, A. Iqbal, S. Ahmad, H. Ali, P. Fu. Microb. Pathog.**114,** 116-123(2018).
34. M. Dembek, S. Bocian, B. Buszewski. Molecules **27,** 968 (2022).
35. L. Xu, W. Li, Q. Shi, H. Li, Z. Yang, D. Liao, L. Li, X. Yang, J. Zhang. J. Photochem. Photobiol. B, Biol. **196,** 111502(2019).
36. P. Boomi, R.M Ganesan, G. Poorani, H. Gurumallesh, S. Ravikumar, J. Jeyakanthan. Mater. Sci. Eng. C **99,** 202-210 (2019).
37. P.R More, S. Pandit, A.D Filipps, G. Franci, I. Mijakovic, M. Galdiero. Microorganisms **11**, 369 (2023).
38. M.G Gallardo, U. Eckhard, L.M Delgado, Y.J.D.D.R Puente, M.H Nogues, F.J Gil, R.A Perez. Bioact. Mater. **6**, 4470-4490 (2021).
39. Z. Yu, Q. Li, J. Wang, Y. Yu, Y. Wang, Q. Zhou, P. Li. Nanoscale Research Lettes. **15**,115 (2020).
40. Z. Bedlovicova, I. Srapac, M. Balaz, A. salayova. Molecules **25,** 3191 (2020).

41. S.B Kedare, R.P Singh. J Food Sci Technol **48,** 412-422 (2011).
42. F. Shahidi, Y. Zhong. J. Func. Foods **18,** 757-781 (2015).
43. S. Baliyan, R. Mukerjee, A. Priyadarshini, A. Vubhuti, A. Gupta, R.P Pandey, C.M Chang. Molecules **27,** 1326 (2022).
44. N. Bloise, S. Strada, G. Dacarro, L. Visai. Int J Mol Sci. **23**, 7683 (2022).
45. A.A Dayem, M.K Hossian, S.B Lee, K. Kim, S.K Saha, G.M Yang, H.Y Choi, S.G Cho. Int J Mol Sci. **18** ,120 (2017).
46. G Kah, R. Chandran, H. Abrahamse. Cells. **12**, 2012 (2023).
47. S.A.S Sakinah, S.T Handayani, L.P.A Hawariah. Cancer Cell Int. **7**, 4 (2007).
48. N.A Badroon, N.A Majid, M.A Alshawsh. Nutrients. **12**,1757 (2020).

Figures

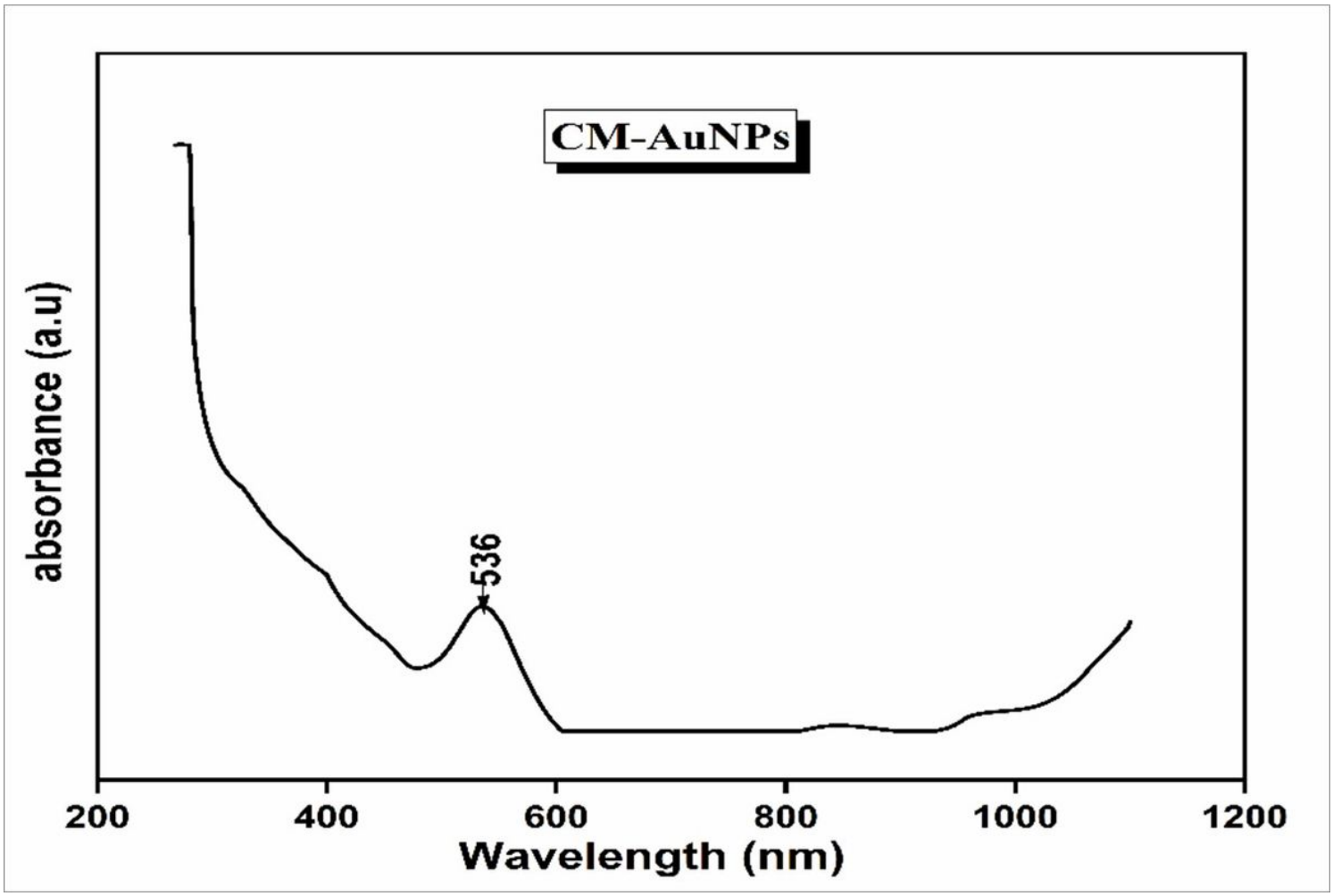

Figure 1

UV-vis spectral profile of bio-synthesized CM-AuNPs

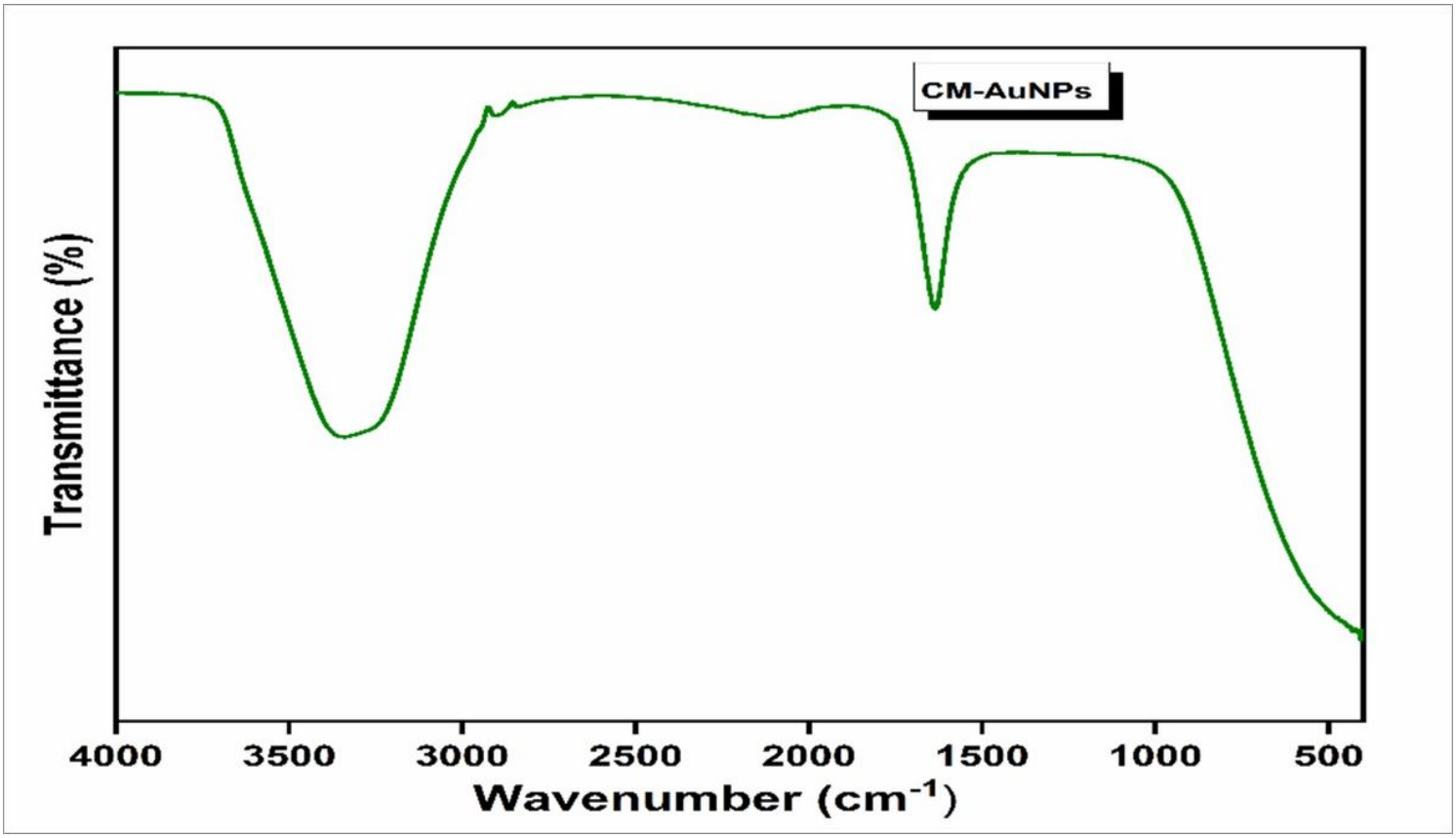

Figure 2

FT-IR graphical representation of bio-synthesized CM-AuNPs.

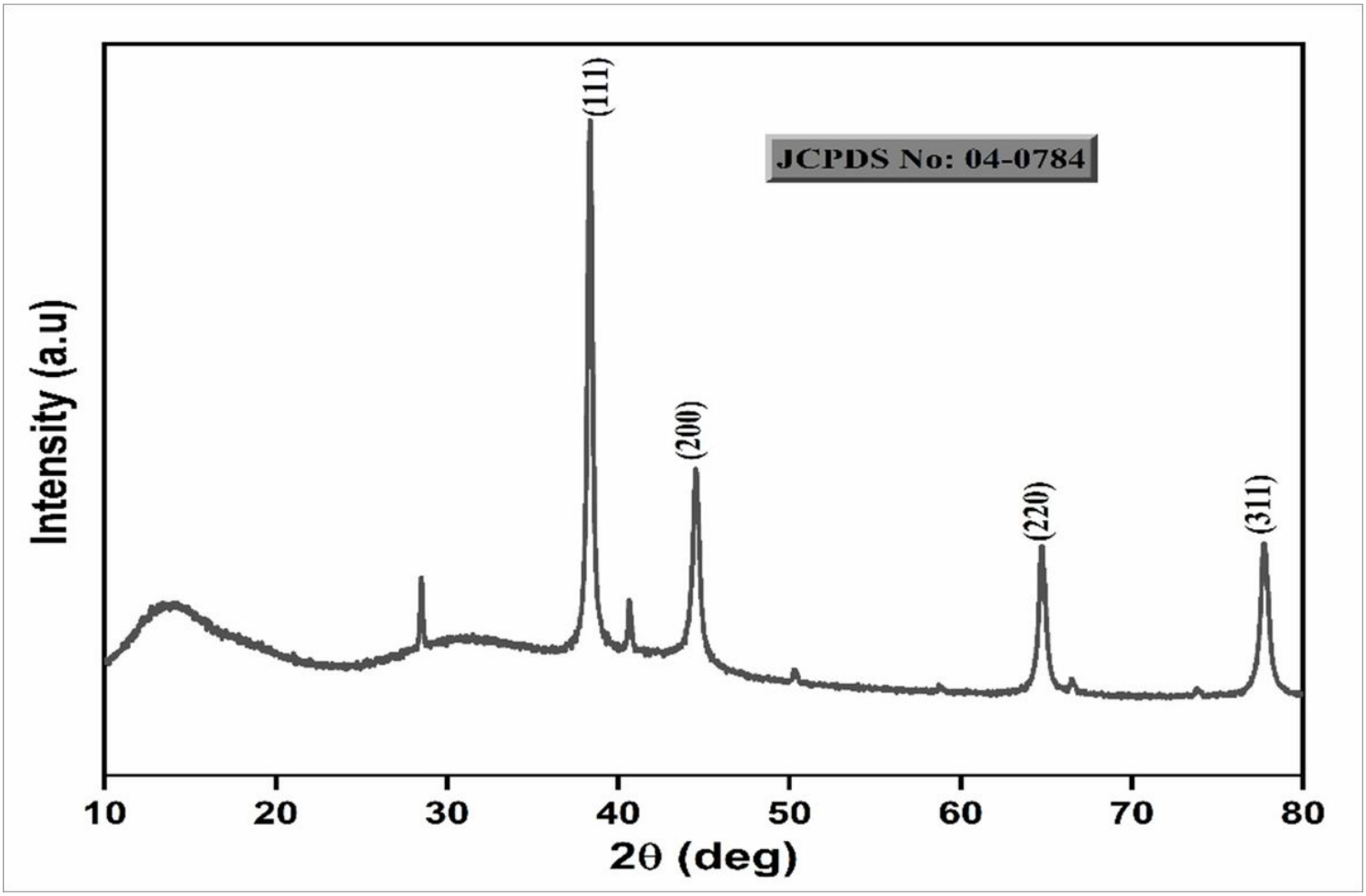

Figure 3

Powder XRD profile of bio-synthesized CM-AuNPs

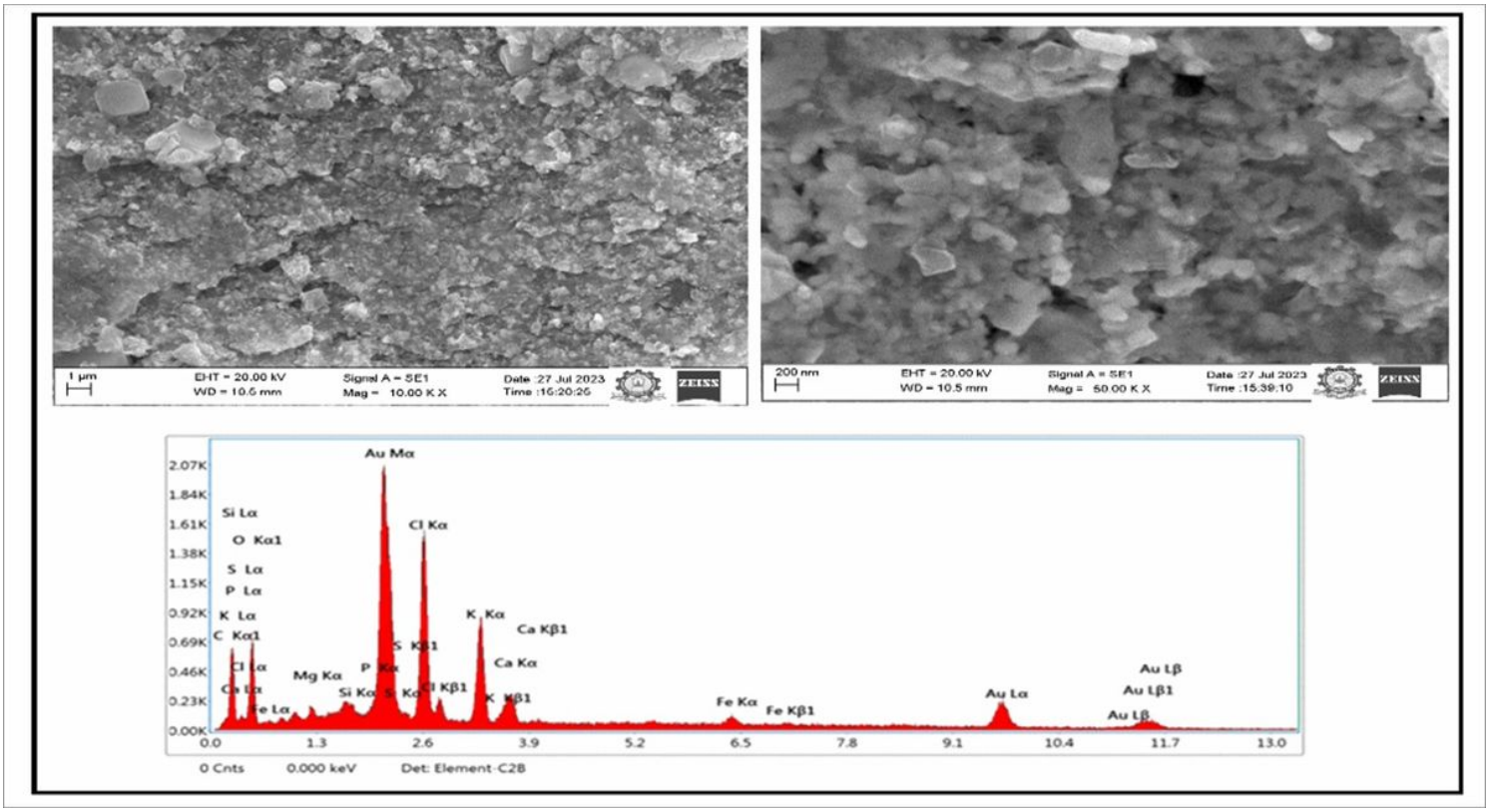

Figure 4

HR-SEM and EDAX profile of CM- AuNPs various scale.

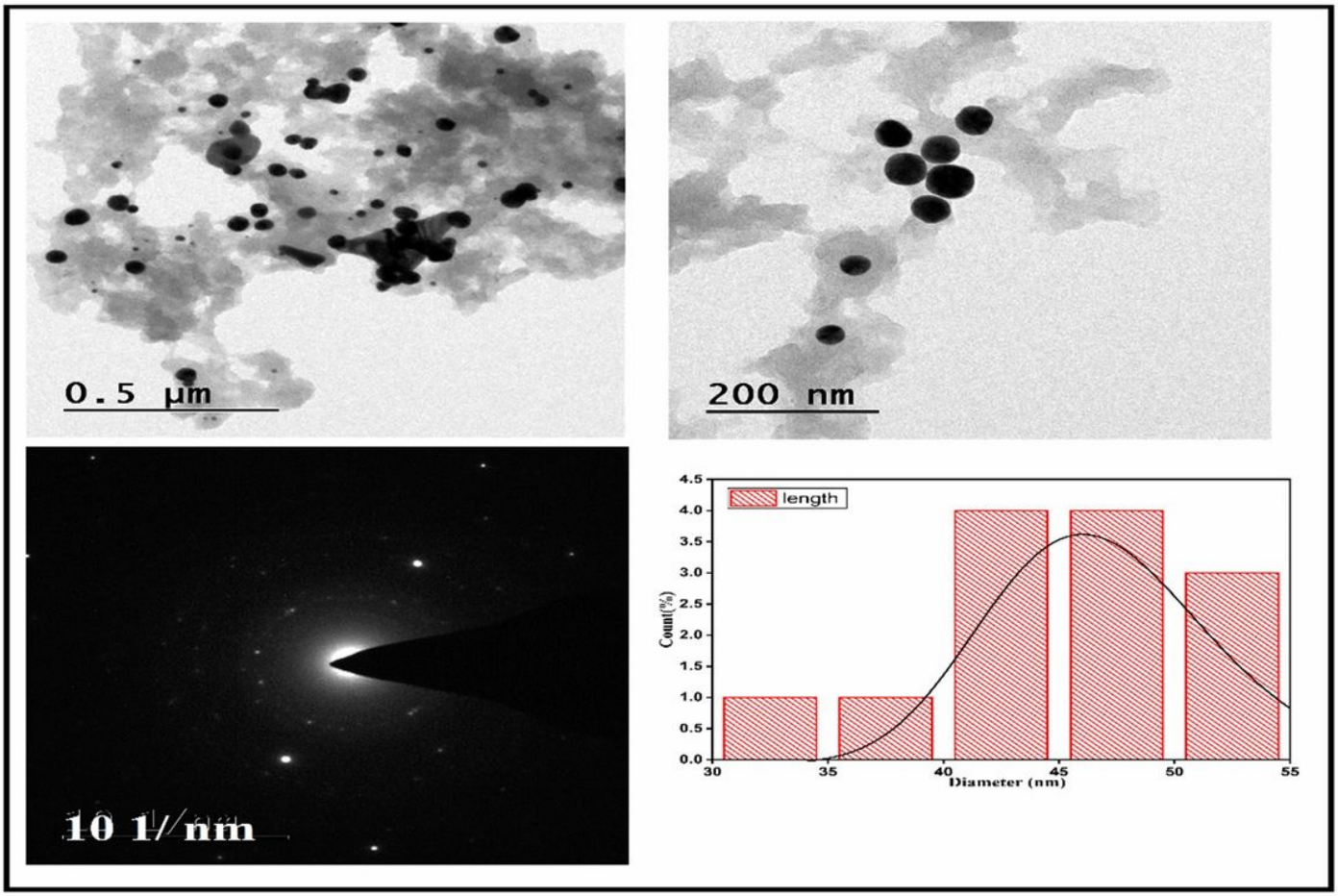

Figure 5

HR-TEM and SAED pattern of CM-AuNPs

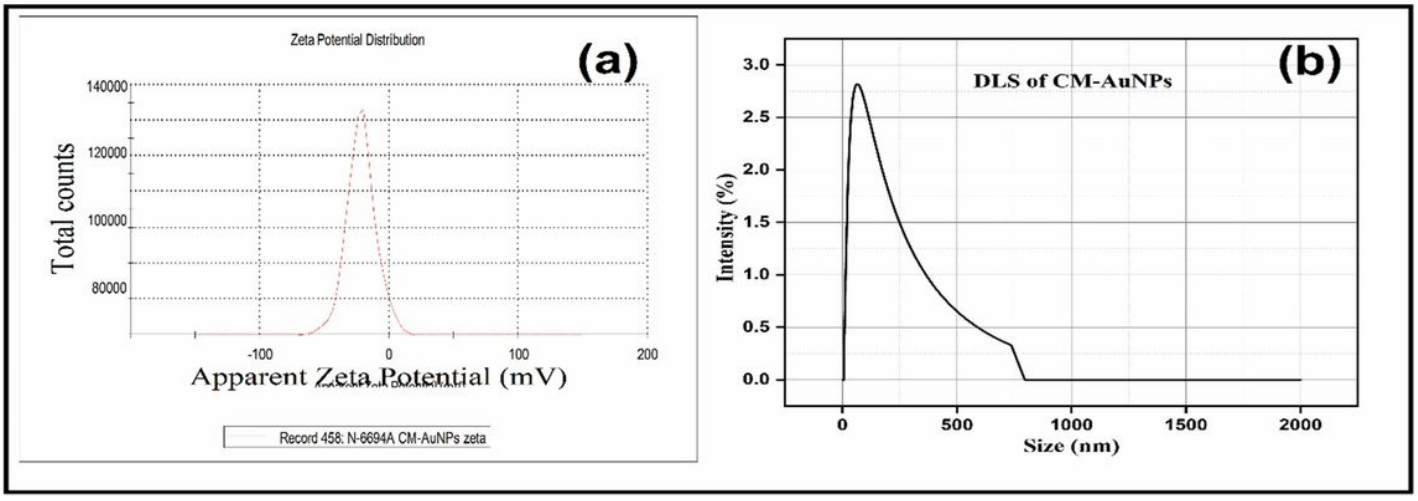

Figure 6

(a) DLS profile of CM-AuNPs and (b) - Zeta potential profile.

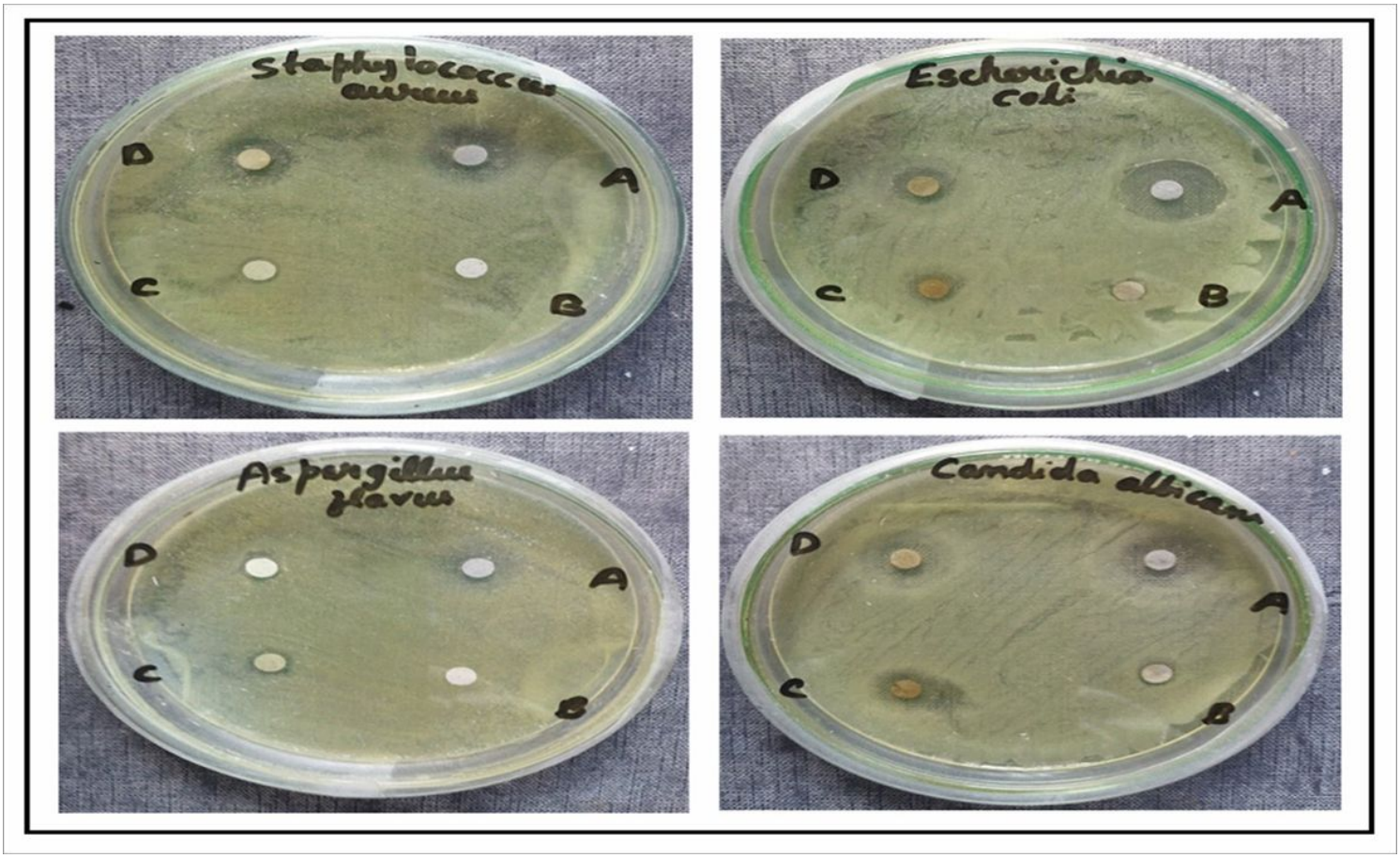

Figure 7

anti-microbial activity of *S.aureus , E.coli, A.flavus and C.albicans.*

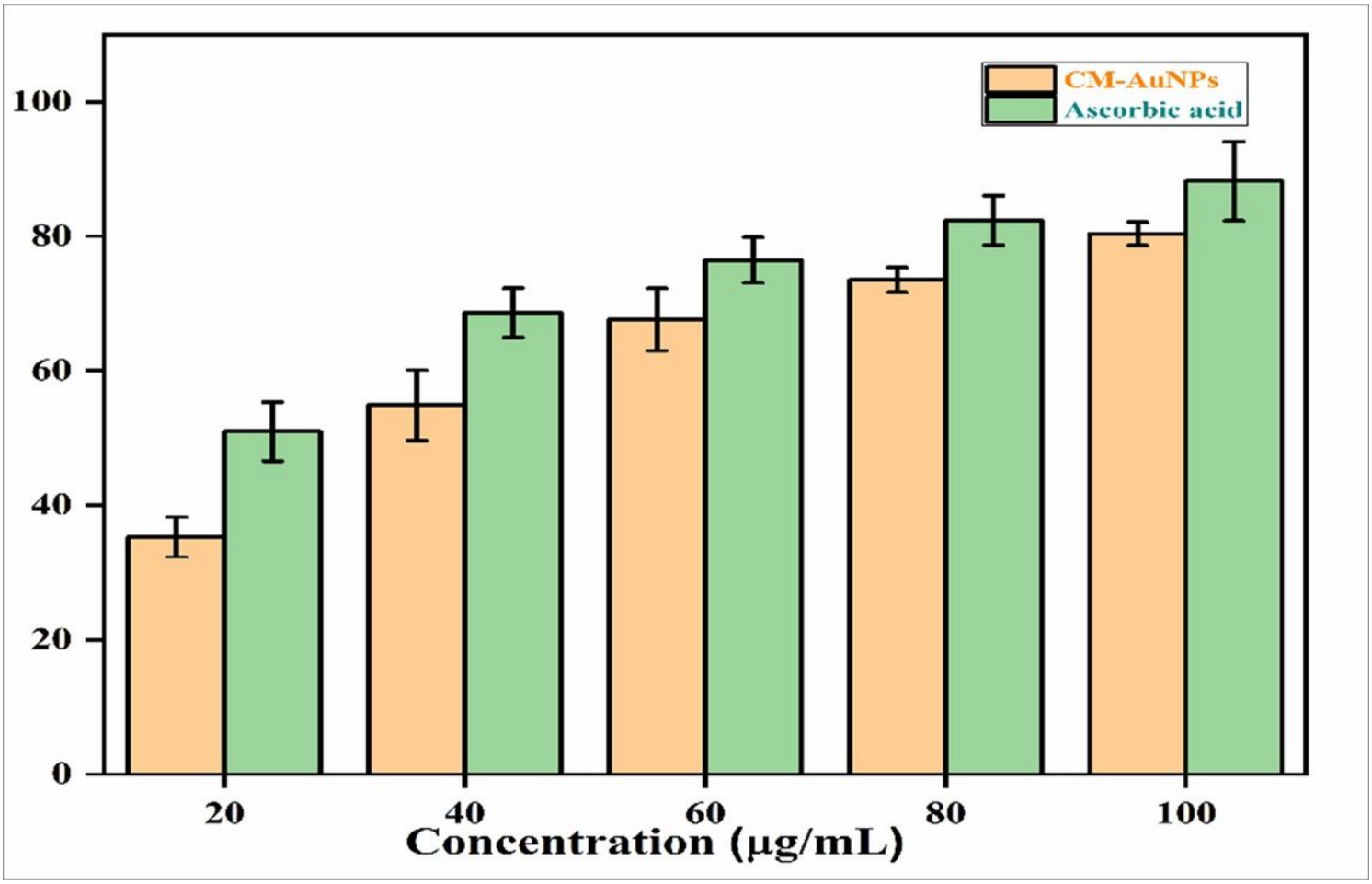

Figure 8

anti-oxidant activity graph of CM-AuNPs.

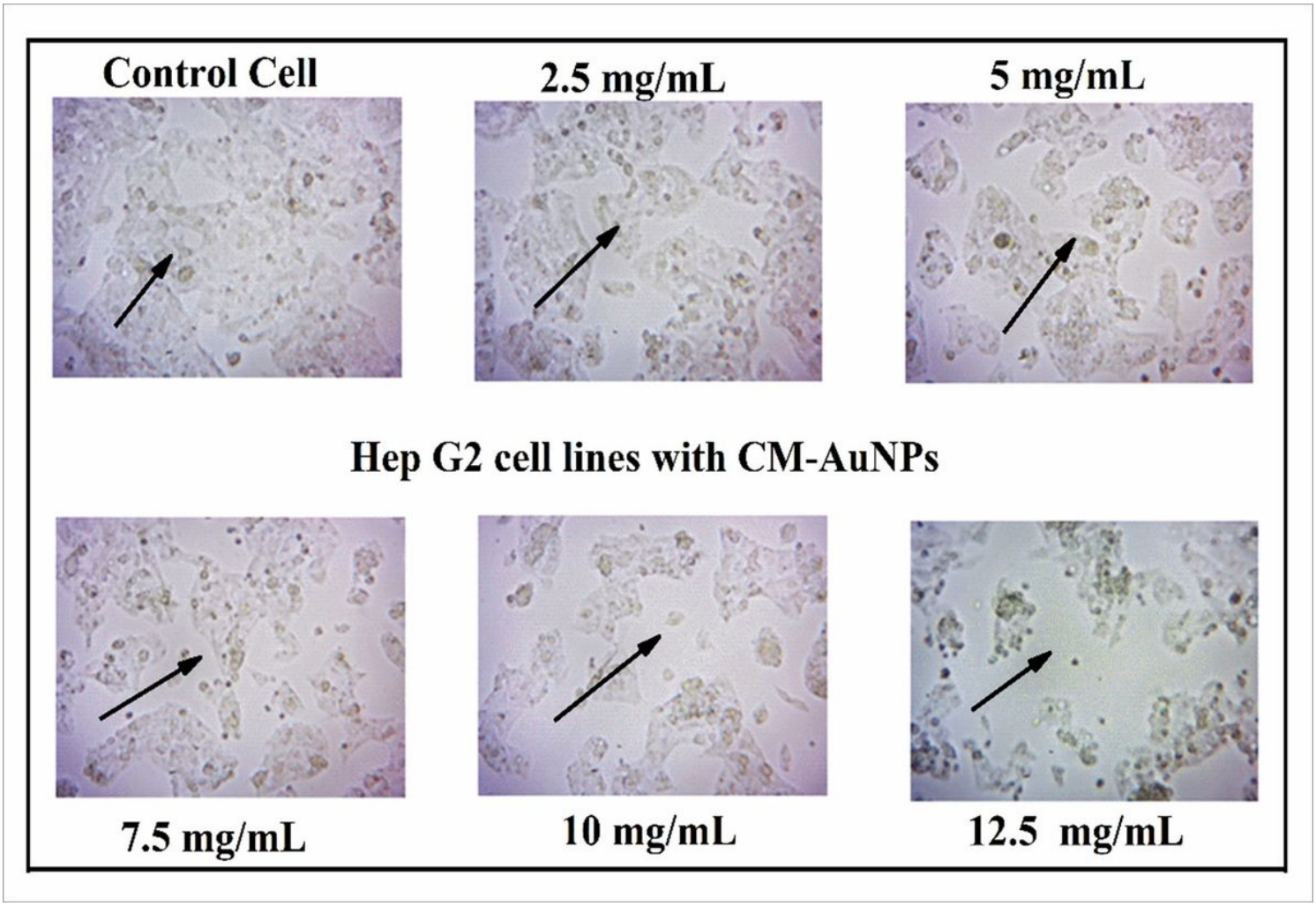

Figure 9

Images of various concentrations of CM-AuNPs used as anti-cancer activity against Hep G2 cancer cell lines.

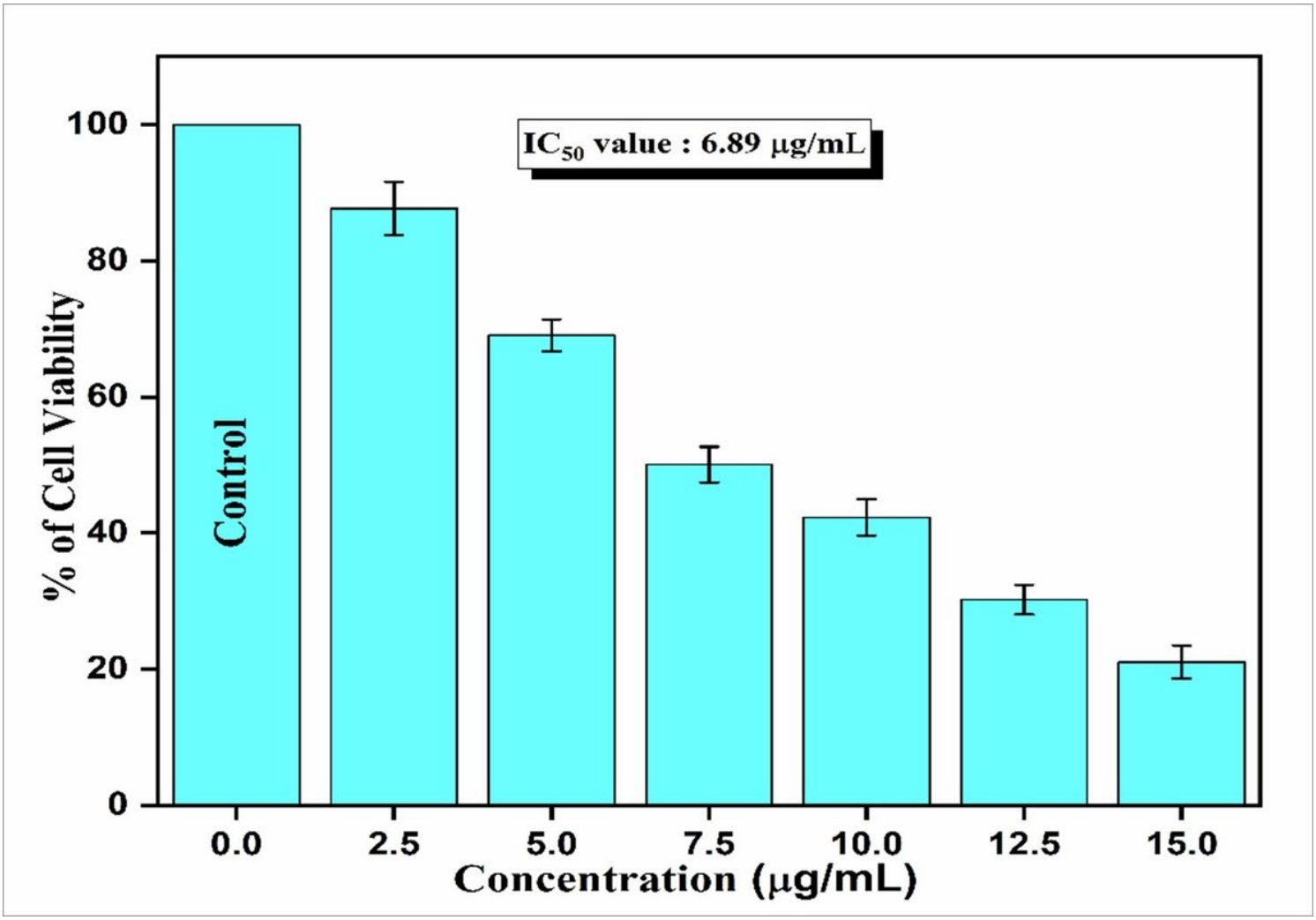

Figure 10

Cell viability graph representation of CM-AUNPs

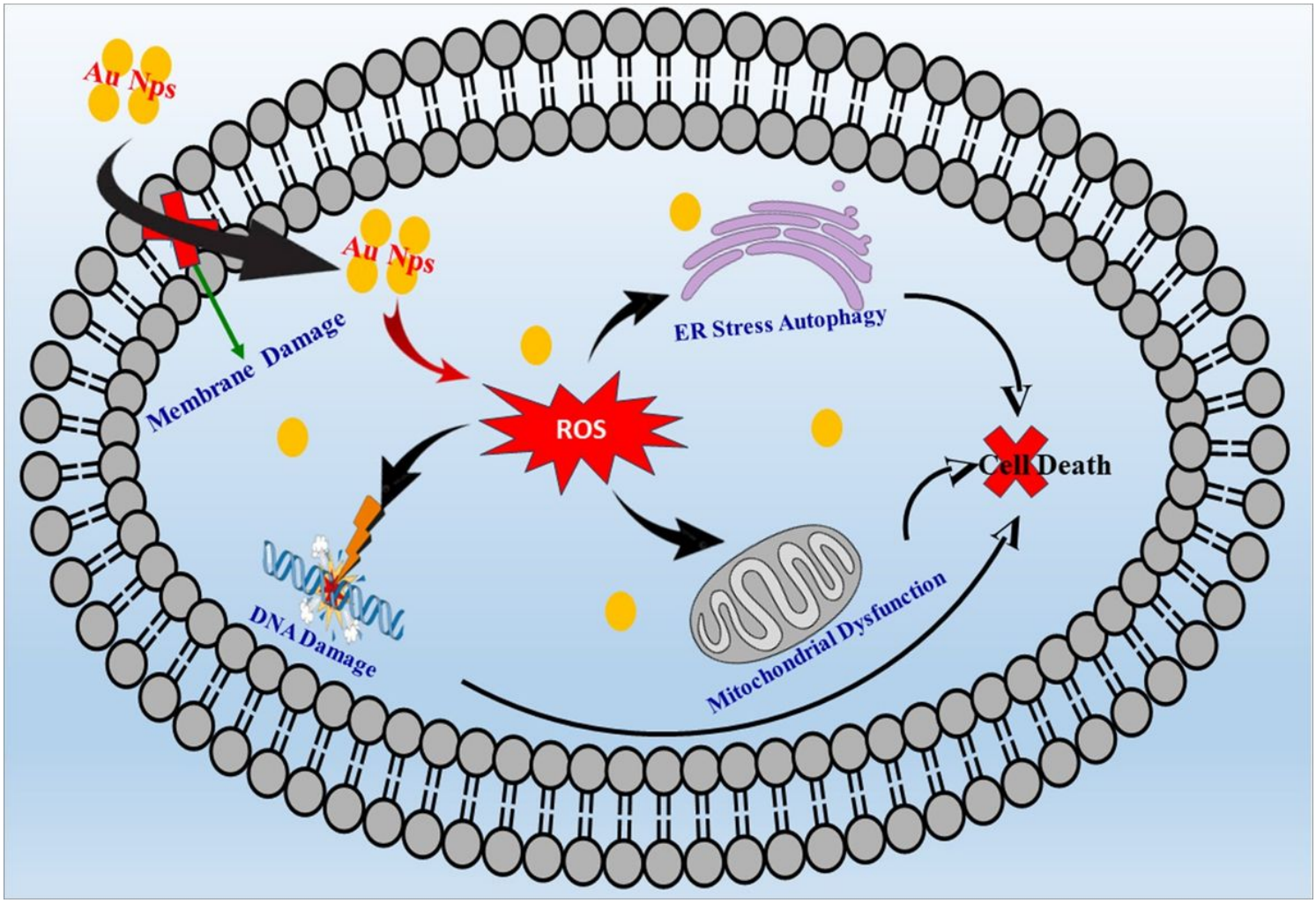

Figure 11

Anti-microbial and anti-cancer Mechanistic explanation diagram of CM-AuNPs